HHS Public Access

Author manuscript

Acad Radiol. Author manuscript; available in PMC 2019 January 01.

Published in final edited form as:

Acad Radiol. 2018 January ; 25(1): 74–81. doi:10.1016/j.acra.2017.08.008.

Robotically Assisted Long Bone Biopsy under MRI Imaging: Workflow and Preclinical Study

Kevin Cleary[a], **Sunghwan Lim**[b], **Changhan Jun**[b], **Reza Monfaredi**[a], **Karun Sharma**[a], **Stanley Fricke**[b], **Lu Vargus**[a], **Doru Petrisor**[a], and **Dan Stoianovici**[b]

[a]Children's National Health System, Sheikh Zayed Institute for Pediatric Surgical Innovation, 111 Michigan Avenue, Washington, DC, 20010

[b]Johns Hopkins University, Brady Urological Institute, Urobotics Laboratory, 5200 Eastern Ave, Baltimore, MD 21224

Structured Abstract

Rationale and Objectives—Our research team has developed an MRI compatible robot for long bone biopsy. The robot is intended to enable a new workflow for bone biopsy in pediatrics under MRI imaging. Our long-term objectives are to minimize trauma and eliminate radiation exposure when diagnosing children with bone cancers and bone infections. This article presents our robotic systems, phantom accuracy studies, and workflow analysis.

Materials and Methods—This section describes several aspects of our work including the envisioned clinical workflow, the MRI compatible robot, and the experimental setup. The workflow consists of five steps and is intended to enable the entire procedure to be completed in the MRI suite. The MRI compatible robot is MR Safe, has 3 degrees of freedom, and a remote center of motion mechanism for orienting a needle guide. The accuracy study was done in a Siemens Aera 1.5T scanner with a long bone phantom. Four targeting holes were drilled in the phantom.

Results—Each target was approached twice at slightly oblique angles using the robot needle guide for a total of eight attempts. A workflow analysis showed the average time for each targeting attempt was 32 minutes, including robot setup time. The average 3D targeting error was 1.39 mm with a standard deviation of 0.40 mm. All of the targets were successfully reached.

Conclusion—The results showed the ability of the robotic system in assisting the Radiologist to precisely target a bone phantom in the MRI environment. The robot system has several potential advantages for clinical application, including the ability to work at the MRI isocenter and serve as a steady and precise guide.

Corresponding author: Kevin Cleary, kcleary@childrensnational.org.
Kevin Cleary, PhD, Technical Director, Bioengineering Initiative, The Sheikh Zayed Institute for Pediatric Surgical Innovation, Children's National Health System, 6th Floor Main Hospital, Room M7735, 111 Michigan Ave., N.W, Washington, D.C 20010, Office Phone: 202-476-3809, Cell Phone: 202-309-9582, kcleary@childrensnational.org

Keywords

Robotics; MRI; long bone biopsy; workflow; MR Safe

Section 1: Introduction

This paper describes our work in developing an MRI compatible robot for long bone biopsy in pediatrics. The robot is intended to enable a novel clinical workflow for image-guided bone biopsy with the goals of minimizing trauma and eliminating radiation exposure in children with bone cancers and bone infections.

Bone pain is a common complaint in children. It can be caused by benign etiologies such as bone infection or malignant etiologies such as bone tumor. Typically, pediatric patients present with symptoms including pain, tenderness, or reluctance to bear weight or use the affected limb. Fevers can be seen in patients with both infections and cancers. Conventional radiographs may be normal, especially early in the course of a disease. MRI is often used to aid in the diagnosis due to its improved soft tissue, marrow, and joint space resolution. The MRI appearance of infectious and neoplastic bone pathology can overlap and sometimes may be indistinguishable. However, clinical management and treatment of these etiologies is quite different.

Osteomyelitis is inflammation of bone caused by infection with bacterial or fungal organisms. Over 50% of reported cases are seen in pre-school age children and are usually caused by acute hematogeous spread form symptomatic or asymptomatic bacteremia [1]. Accurate and timely diagnosis of bone infection and the infecting organism is critical for optimal therapy as treatment consists of long term antibiotics, with surgical debridement in advanced cases. As noted in a recent review article of pediatric osteomyelitis, “a delay in the diagnosis of pediatric acute and subacute haematogenous osteomyelitis can lead to potentially devastating morbidity [2].”

Malignant bone cancers are the fourth most common pediatric solid tumors after central nervous system tumors, sarcomas, and retinoblastoma [3]. The most common malignant bone tumors in children include osteosarcoma and Ewing sarcoma [4] and accurate histologic diagnosis is a key for treatment planning. Treatment for bone tumors is complex and can involve various combinations of chemotherapy, radiation therapy, surgical resection, and even amputation. Before the appropriate treatment plan can be implemented, a tissue diagnosis is often needed.

If a suspicious focal mass or area of bone marrow abnormality is seen on MRI, and the diagnosis can not be made through clinical history, examination, laboratory tests and imaging findings, a biopsy is frequently needed for pathological evaluation and definitive tissue diagnosis, which forms the basis for appropriate treatment. The biopsy can be performed in the operating room by the orthopedic surgery team, or under X-ray or CT guidance in the Radiology suite, necessitating additional anesthesia and open surgery in one situation, and exposure to ionizing radiation in the other. In both situations, significant additional time is required to achieve a definitive tissue diagnosis. In addition, bone and

marrow lesions may be difficult to directly visualize during surgery or with x-ray and CT imaging, increasing the possibility of missed sampling and inaccurate diagnosis. If an MRI-guided, targeted bone biopsy could be performed immediately following MRI diagnosis of an abnormality in the MRI suite using robotic assistance as described here, trauma and radiation exposure to the patient could be minimized, while precise sampling could be obtained. An alternative would be to use MRI fusion techniques outside of the MRI suite, bringing MRI information to the ultrasound or CT imaging setting [5].

The paper is organized as follows. Related work in MRI compatible robotics is presented in Section 2. In Section 3, Materials and Methods, we then describe the new proposed clinical workflow, the MRI compatible robot we developed, and our experimental setup. In Section 4 we present the results of a workflow timing analysis and targeting accuracy study under MRI using a long bone phantom. Conclusions are given in Section 5.

Section 2: Related Work

While many groups have developed prototype MRI compatible robots, there are no commercial systems for needle placement available, and research efforts continue at several sites worldwide. Review articles describing MRI compatible robotic systems and the associated challenges include the articles by Tsekos et al. [6] and Gassert et al. [7].

While MRI compatible robots could be categorized in many different ways, one way is through the four classifications shown in Table 1. For each classification, subcategories are also listed, and some of the representative literature is summarized below. The table is not meant to be exhaustive, but rather to give an overview of the field.

Clinical application

Two distinct clinical applications are needle-based procedures and rehabilitation applications. Moreira et al. [8] developed a 9 DoF MRI compatible robot called MIRIAM (Minimally Invasive Robotics In An Magnetic Resonance Imaging environment) to steer and fire a biopsy needle during the prostate biopsy procedure. This robotic system consists of a 5 DoF parallel robot driven by piezoelectric motors to position the needle guide and a 4 DoF needle driver to insert, rotate, and fire the biopsy gun. Stoianovici et al. [9] presented a system for endorectal prostate biopsy. This system was used to orient the biopsy needle guide during the biopsy procedure. Authors reported promising results for both in vitro and in animal studies. Recently the same group reported the clinical application of an MR Safe robot for prostate biopsy [10]. For rehabilitation, Estévez et al. [11] used an MRI-compatible arm robot in healthy subjects to define the brain network activated while performing active and passive elbow movements, and to test the reproducibility of this activation over time. Yap et al. [12] present the design, fabrication and evaluation of a wearable soft robotic glove for hand rehabilitation were presented in. The glove consists of a set of soft pneumatic actuators made of silicon elastomers and was used for brain activity study during hand rehabilitation.

Mounting method

An MR robot could be mounted on the patient body or on the moving MRI table. Monfaredi et al. [13] developed a 4 DoF patient-mounted MRI-compatible robot for shoulder arthrography and showed the robot could be stably mounted using straps. Hata et al. [14] developed a patient-mounted robot for cryoablation. An average targeting error of 2.0 mm for needle-point placement experiments was reported using a gelatin phantom. Melzer et al. [15] described the INNOMOTION bed-mounted robot for percutaneous image-guided interventions. Franco et al. [16] developed a bed-mounted robot for use in MRI-guided laser ablation of liver tumors and showed below 5 mm targeting error in phantom study.

Actuation method

Van den Bosch et al. [17] employed pneumatic and hydraulic actuation to develop a robotic system for prostate seed implantation with automated needle insertion. Su et al. [18] presented a 6 DoF robot with piezoelectric motors for prostate therapy under MRI, consisting of a 3 DoF needle driver module (cannula translation and rotation and stylet translation) and a 3 DoF Cartesian motion stage. The robotic system for long bone biopsy described in this paper is a needle-guide robot that is bed-mounted, uses pneumatic actuation [19], and is MR Safe [20].

MR classification

The American Society for Testing and Materials (ASTM) has developed standard F2503 to classify devices for the MRI environment. In the United States, compliance to these standards is required for medical device regulatory clearance by the Food and Drug Administration (FDA). MR Safe is a device that poses no known hazards in all MR environments. MR conditional is a device that has been demonstrated to pose no known hazards in a specified MR environment with specified conditions of use such as field strength. MR conditional devices include the pneumatic stepper motor of Chen et al. [21] and the prototype robot for transcranial focused ultrasound surgery of Price et al. [22]. MR safe devices include the prostate biopsy robots from Stoianovici et al. [9], [10] and Schouten et al. [23].

Section 3: Materials and Methods

In this section, we describe several aspects of our work: 1) the envisioned clinical workflow with the MRI compatible robot; 2) the MRI compatible robot that we developed; and 3) the setup for the experimental accuracy results using a Siemens 1.5T MRI and a long bone phantom.

Section 3.1: Clinical Workflow

The proposed clinical workflow using the robot is shown in Figure 1. The workflow consist of 5 steps as follows:

Step 1. Positioning of patient and robot. The patient is positioned on the MRI table in the usual manner. The robot is then mounted onto the table between the patient’s legs

so that the needle-guide is located at the skin entry point. MR imaging coils are placed around the leg and the robot. The robot is already turned on and homed.

Step 2. MR imaging and trajectory planning. Standard MR diagnostic imaging sequences for bone infections (or tumors) are obtained, including multi-planar T1/T2 weighted and contrast enhanced sequences. The Interventional Radiologist reviews the images and selects bone target point as well as the skin entry point which defines the trajectory for the needle along a safe path that avoids critical structures such as blood vessels and nerves.

Step 3. Robot registration and alignment. The robot has built-in fiducials for registering the robot coordinate system with the image coordinate system. Once the robot is registered, it is commanded to align the end-effector along the safe trajectory defined in Step 2.

Step 4. Confirmation of trajectory. An MRI-visible fiducial of the same size as the bone biopsy drill is placed through the needle-guide and the tip is positioned on the “skin”. A confirming set of MR images are taken to verify that the trajectory of the fiducial matches the desired trajectory. This step may be eliminated when the reliability of robotic needle-guidance is documented in clinical experiments. This has the potential to reduce the procedure time.

Step 5. Insert bone biopsy drill and take sample. The Interventional Radiologist manually drives the biopsy drill to the target. The depth indicator on the drill is set based on the planned trajectory. Confirming images may be acquired with the drill in place. The bone samples are obtained as usual.

Section 3.2: MRI Compatible Robot

An MR Safe (ASTM F2503) robot has been developed with 3 degrees of freedom (DoF) [20]. The robot mounts on the MRI table and its location is manually positioned with 4 degrees of adjustment (DoA). It orients a needle-guide about two orthogonal axes intersecting at a point located below the guide using a Remote Center of Motion (RCM) mechanism [24], [25]. The axes are actuated with two PneuStep motors [19] coaxially located on the robot base [9]. The needle is inserted manually through the guide. The depth of needle insertion is set by a third PneuStep motor located remotely. Before the insertion, this pre-adjusts the location of a depth stop along the barrel of the needle [9].

The robot is electricity free, uses air pressure for actuation, light for the position sensors, and is entirely made of nonconductive, non-metallic, and nonmagnetic materials. Accordingly, the robot is MRI-Safe according to ASTM F2052, F2213, and F2182 based on the scientific rationale [20]. The needle-guide, which comes in direct contact with the patient, is built of certified biocompatible material (ISO-10993). The bore of the needle-guide can be made to accommodate various needles. The prototype was built for the MRI-Conditional Invivo 15100 bone biopsy drill (Invivo, Philips Healthcare, The Netherlands).

The robot includes high contrast MRI markers for registration (filled with MR-Spots contrast, Beekley, Bristol, CT). A custom image-to-model registration algorithm and image-guided control software was developed. Bench tests of stiffness and motion accuracy, imager

and electromagnetic compatibility tests, and image-guided targeting accuracy tests have been performed [20]. These tests showed the robot does not interfere with the MRI images and is highly accurate on the bench.

Section 3.3: Experimental Setup: Targeting Accuracy

We evaluated the accuracy of the system in a 1.5T Siemens Aera scanner at Children's National Medical Center. The experimental setup is shown in Figures 2A to 2D below. Figure 2A shows the robot mounted to the table with a long bone phantom between the imaging coils. A custom-built table mount (purple frame in figure) was anchored to the mounting slots in the Siemens table and the robot was attached to this mount. Figure 2B shows the coils removed with a long thin fiducial in the needle guide. This fiducial was used to confirm targeting accuracy as described below. Figure 2C shows the same configuration as Figure 2A but with the robot at isocenter. Since the robot is made entirely of non-metallic materials and has no electrical parts, it presents no interference when scanning. Therefore, if required by the clinical application, the robot could be manipulating an instrument at isocenter while scanning in real-time. Figure 2D is similar to Figure 2B but taken from the right side and shows the planned positioning of the robot where it could go between the legs of the patient.

A long bone phantom was created by placing a femur phantom model (Sawbones, Pacific Research Laboratories) in a gelatin mixture inside a long cylindrical tube (Figure 3A). A small opening was cut at the top of the tube to allow access for targeting experiments. Small holes were drilled in the bone along this opening as targets. Four holes were used for this study and each hole was targeted twice (Figure 3B).

The experimental procedure followed the proposed clinical workflow show in Figure 1 with some modifications. For each of the four targets:

The robot was manually positioned near the target of interest. This was accomplished by loosening the plastic retaining screws on the passive base and moving the robot by hand until the RCM point of the robot (located slightly below the needle guide) was near the desired entry site of the phantom.

The MRI table was moved into the scanner with the center of our region of interest at the isocenter of the magnet. A series of MRI scans were done using 3D T1 Vibe sequence. The following T1 vibe parameters were used for the pneumatic bone biopsy: TR=8.85ms, TE=1.35 ms, Fov= 380mm, Matrix =320×320, Slice thickness=1.2 mm, Gap=1.24mm, Flip angle=14.5 deg, and IPAT=3.

DICOM images were read into the image-guidance and robot control workstation (developed by our group). These were used for robot-to-image registration and target selection.

The workstation software confirms target point to be within the robot workspace. The robot is then commanded to align the end-effector to point at the target point. The needle insertion depth is also computed.

An acrylic trocar of the same diameter and length as the biopsy trocar (4.87 mm, length 135 mm) with a pencil point was inserted through the needle-guide toward the target. The depth of insertion was controlled by an o-ring on the acrylic trocar whose position was set by the third stage of the robot system as described in Section 2.2. The acrylic trocar was used as the metal trocar resulted in too much artifact to accurately segment and precisely evaluate its point location for this accuracy study.

A confirming MRI scan was then done to evaluate the actual tip position as described in the results section next.

Section 4: Results

Workflow results

As part of this study, we did an analysis of the time required for each of the eight targeting attempts. That analysis is shown in Table 2 on the next page. The precise times were extracted from time stamps in the DICOM files and the other times were estimated. All times shown are in minutes. As can be seen in the table, the average time for each targeting attempt was 32.37 minutes, with a standard deviation of 1.46 minutes. These results lead us to believe that with some practice we could complete a clinical case in 60 to 90 minutes, allowing for variability in the time required for patient positioning. This amount of time would be within the range allocated for MRI procedures at our institution, thus indicating that our bone biopsy procedure would not interrupt normal clinical workflow.

Targeting Experiment Results

Four targets were used for this feasibility study. Two targeting attempts were made for each target on two different days. The targeting attempts were done by one of the engineers working on the project. All of the targeting attempts were made at slightly oblique angles as shown in the table below, illustrating the ability of the robot to help with oblique trajectories, which can be challenging. An error analysis was then completed to compute two values: the perpendicular distance from the trocar path to the target and the distance from the trocar point to the target. The error analysis was done from the confirming MRI images as follows:

1. The center of the target hole was first determined. The target was semi-automatically segmented using a marching cubes algorithm [26]. Next, to find the center of the target, a hemisphere was registered to the segmented target surface using an iterative closest point algorithm [27].
2. The long axis of the trocar was next determined. The trocar was semi-automatically segmented using a marching cubes algorithm. The center axis of the segmented trocar was then estimated using principal component analysis [28]. To estimate the point position of the trocar, the 3D computer model from computer aided design (CAD) of the trocar was registered to the segmented trocar model by aligning the two center axes. The position along the axes was manually adjusted by sight until the two models were superimposed (image-to-model registration) (Figure 4A).

3. The 2D error was computed as the shortest distance between the target point and the estimated needle axis

4. 3D error was computed as the distance between the target point and the point of the trocar CAD model (Figure 4B)

5. The results for the 8 trials are shown in Table 3 on the next page. The target depth is shown, followed by the two needle insertion angles, along with the 2D and 3D errors. In the needle insertion angles, negative values indicate a medial or superior direction, while positive values indicate a lateral or inferior direction. The maximum 2D error was 1.72mm and the maximum 3D error was 1.89 mm. The average 2D error was 1.25 mm and the average 3D error was 1.39 mm. The standard deviation was 0.39 mm for 2D and 0.40 mm for 3D.

Section 5: Conclusions

In this paper, we presented a novel robotic system for precisely placing a bone biopsy needle guide under MRI. We carried out a workflow analysis and targeting accuracy study.

The results show that the robotic system can be used to accurately place a bone biopsy drill guide in a phantom long bone model under MR imaging. All of the targeting trials were completed with no problems and no system failures were observed with the robot.

The robotic system has several potential advantages for clinical applications:

1. It can serve as a steady and precise needle guide for the Interventional Radiologist

2. The position and orientation of the trocar can be verified before inserting into the leg if desired.

3. The robot can work at the magnet isocenter as well as provide improved ergonomics for the operator.

4. The robot should allow for decreased tissue trauma resulting from a single accurate needle pass as compared to multiple passes needed to adjust the trajectory by free hand.

5. The single pass should also allow for decreased total procedure anesthesia time. Moreover, in the future, if the diagnostic imaging and biopsy could be completed in the same setting as outlined here, it would eliminate the need for a second anesthesia.

In future work, we plan to move to clinical trials at our pediatric hospital, focusing on long bone biopsy of the leg (specifically, the femur and tibia). Although speculative at this time, a clinical MR-compatible robotic system that provides precise and convenient needle placement under MRI guidance could also be useful for other clinical applications such as percutaneous screw and pin placement in treatment of traumatic bone fractures and for needle probe plaecement required to perform thermal ablation of bone and soft tissue

tumors. These types of image-guided percutaneous interventions are currently commonly performed using CT imaging guidance [29]–[32].

Acknowledgments

This research was funded by NIH grant R01CA172244, Pneumatic Robot for MRI-Guided Long Bone Biopsy. The MR Safe robot technology developments were supported in part by awards RC1EB010936 from the National Institute of Biomedical Imaging and Bioengineering, and W81XWH0810221 from the Department of Defense. This research was also supported by the Intramural Research Program of the National Institutes of Health, National Heart, Lung, and Blood Institute, HHSN268200900052C. We would also like to thank the MRI technologist Sheena Badger for her help with the experimental studies.

References

1. Gutierrez K. Bone and joint infections in children. Pediatr. Clin. North Am. 2005; 52(3):779–794. [PubMed: 15925662]
2. Dartnell J, Ramachandran M, Katchburian M. Haematogenous acute and subacute paediatric osteomyelitis: a systematic review of the literature. J Bone Joint Surg. Br. May; 2012 94(5):584–595. [PubMed: 22529075]
3. Vasudevan V, et al. Pediatric solid tumors and second malignancies: characteristics and survival outcomes. J Surg. Res. May; 2010 160(2):184–189. [PubMed: 19765728]
4. National Cancer Institute. [Accessed: 10-Dec-2016] Cancer in Children and Adolescents. National Cancer Institute. [Online]. Available: https://www.cancer.gov/types/childhood-cancers/child-adolescent-cancers-fact-sheet
5. Siddiqui MM, et al. Comparison of MR/ultrasound fusion–guided biopsy with ultrasound-guided biopsy for the diagnosis of prostate cancer. Jama. 2015; 313(4):390–397. [PubMed: 25626035]
6. Tsekos NV, Khanicheh A, Christoforou E, Mavroidis C. Magnetic Resonance–Compatible Robotic and Mechatronics Systems for Image-Guided Interventions and Rehabilitation: A Review Study. Annu Rev Biomed Eng. 2007; 9(1):351–387. [PubMed: 17439358]
7. Gassert R, Burdet E, Chinzei K. Opportunities and Challenges in MR-Compatible Robotics. Eng. Med. Biol. Mag. IEEE. 2008; 27(3):15–22.
8. Moreira P, et al. The MIRIAM Robot: A Novel Robotic System for MR-Guided Needle Insertion in the Prostate. J Med. Robot. Res. Oct.2016 :1750006.
9. Stoianovici D, et al. MRI-safe robot for endorectal prostate biopsy. IEEEASME Trans. Mechatron. 2014; 19(4):1289–1299.
10. Stoianovici D, et al. MR Safe Robot, FDA Clearance, Safety and Feasibility Prostate Biopsy Clinical Trial. IEEEASME Trans. Mechatron. 2016
11. Estévez N, et al. A reliability study on brain activation during active and passive arm movements supported by an mri-compatible robot. Brain Topogr. 2014; 27(6):731–746. [PubMed: 24718725]
12. Yap HK, Kamaldin N, Lim JH, Nasrallah F, Goh JC, Yeow C-H. A Magnetic Resonance Compatible Soft Wearable Robotic Glove for Hand Rehabilitation and Brain Imaging. IEEE Trans. Neural Syst. Rehabil. Eng. 2016
13. Monfaredi, R., et al. Shoulder-Mounted Robot for MRI-guided arthrography: Accuracy and mounting study; Engineering in Medicine and Biology Society (EMBC), 2015 37th Annual International Conference of the IEEE; 2015. p. 3643-3646.
14. Hata N, et al. Body-mounted robotic instrument guide for image-guided cryotherapy of renal cancer. Med. Phys. 2016; 43(2):843–853. [PubMed: 26843245]
15. Melzer A, et al. INNOMOTION for Percutaneous Image-Guided Interventions. IEEE Eng. Med. Biol. Mag. May; 2008 27(3):66–73.
16. Franco E, Brujic D, Rea M, Gedroyc WM, Ristic M. Needle-Guiding Robot for Laser Ablation of Liver Tumors Under MRI Guidance. IEEEASME Trans. Mechatron. 2016; 21(2):931–944.
17. Van den Bosch MR, et al. MRI-guided robotic system for transperineal prostate interventions: proof of principle. Phys. Med. Biol. 2010; 55(5):N133. [PubMed: 20145293]

18. Su H, et al. Piezoelectrically actuated robotic system for MRI-guided prostate percutaneous therapy. 2015
19. Stoianovici D, Patriciu A, Petrisor D, Mazilu D, Kavoussi L. A New Type of Motor: Pneumatic Step Motor. IEEEASME Trans. Mechatron. Feb; 2007 12(1):98–106.
20. Stoianovici D, et al. MR Safe Remote Center of Motion Bone Biopsy Robot. IEEE Trans. Biomed. Eng. 2016 p. under review.
21. Chen Y, Kwok K-W, Tse ZTH. An MR-conditional high-torque pneumatic stepper motor for MRI-guided and robot-assisted intervention. Ann. Biomed. Eng. 2014; 42(9):1823–1833. [PubMed: 24957635]
22. Price KD, et al. Design and validation of an MR-conditional robot for transcranial focused ultrasound surgery in infants. Med. Phys. 2016; 43(9):4983–4995. [PubMed: 27587029]
23. Schouten MG, Ansems J, Renema W, Bosboom D, Scheenen TW, Fütterer JJ. The accuracy and safety aspects of a novel robotic needle guide manipulator to perform transrectal prostate biopsies. Med. Phys. 2010; 37(9):4744–4750. [PubMed: 20964192]
24. Stoianovici, D., Whitcomb, LL., Anderson, JH., Taylor, RH., Kavoussi, LR. A modular surgical robotic system for image guided percutaneous procedures; International Conference on Medical Image Computing and Computer-Assisted Intervention; 1998. p. 404-410.
25. Stoianovici D, et al. AcuBot: a robot for radiological interventions. IEEE Trans. Robot. Autom. Oct; 2003 19(5):927–930.
26. Lorensen WE, Cline HE. Marching cubes: A high resolution 3D surface construction algorithm. ACM siggraph computer graphics. 1987; 21:163–169.
27. Besl PJ, McKay ND. Method for registration of 3-D shapes. Robotics-DL tentative. 1992:586–606.
28. Pearson K. LIII. On lines and planes of closest fit to systems of points in space. Lond. Edinb. Dublin Philos. Mag. J. Sci. 1901; 2(11):559–572.
29. Barile A, et al. Minimally invasive treatments of painful bone lesions: state of the art. Med. Oncol. 2017; 34(4):53. [PubMed: 28236103]
30. Sciulli RL, Daffner RH, Altman DT, Altman GT, Sewecke JJ. CT-guided iliosacral screw placement: technique and clinical experience. Am. J. Roentgenol. 2007; 188(2):W181–W192. [PubMed: 17242226]
31. Blake-Toker A-M, et al. CT guided percutaneous fixation of sacroiliac fractures in trauma patients. J Trauma Acute Care Surg. 2001; 51(6):1117–1121.
32. Routt MC Jr, Nork SE, Mills WJ. Percutaneous fixation of pelvic ring disruptions. Clin. Orthop. 2000; 375:15–29.

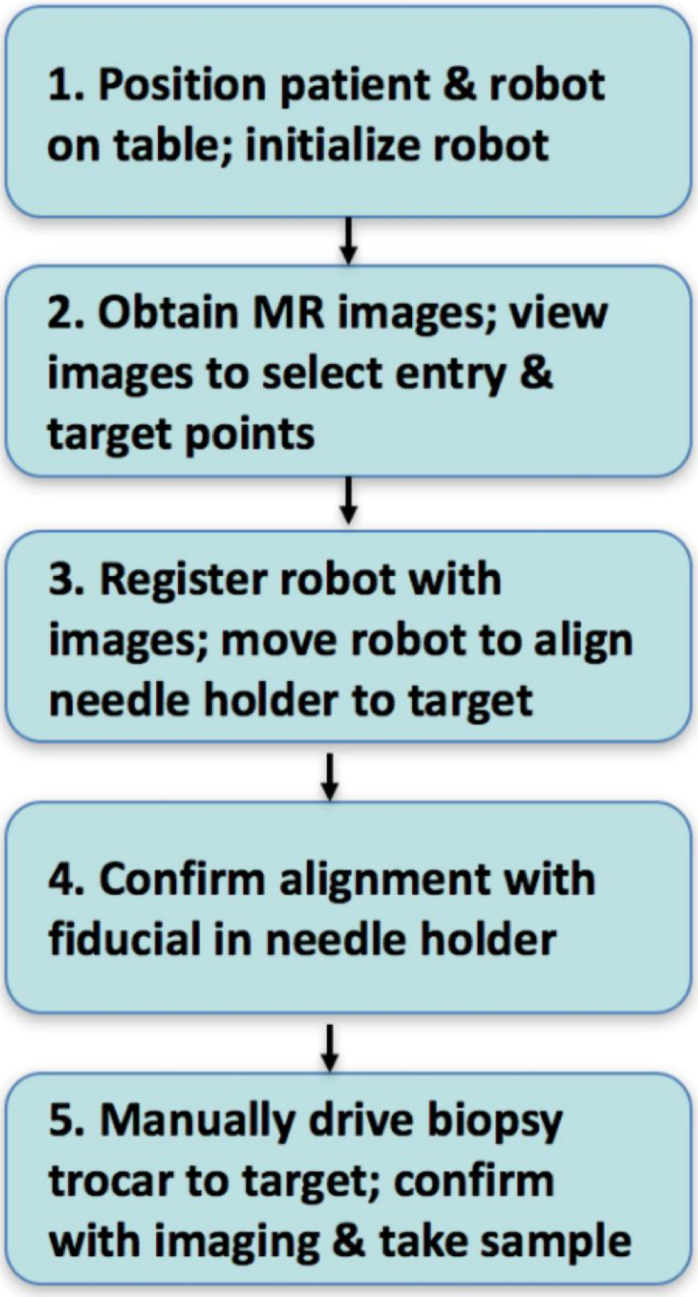

Figure 1.
Proposed clinical workflow

A

B

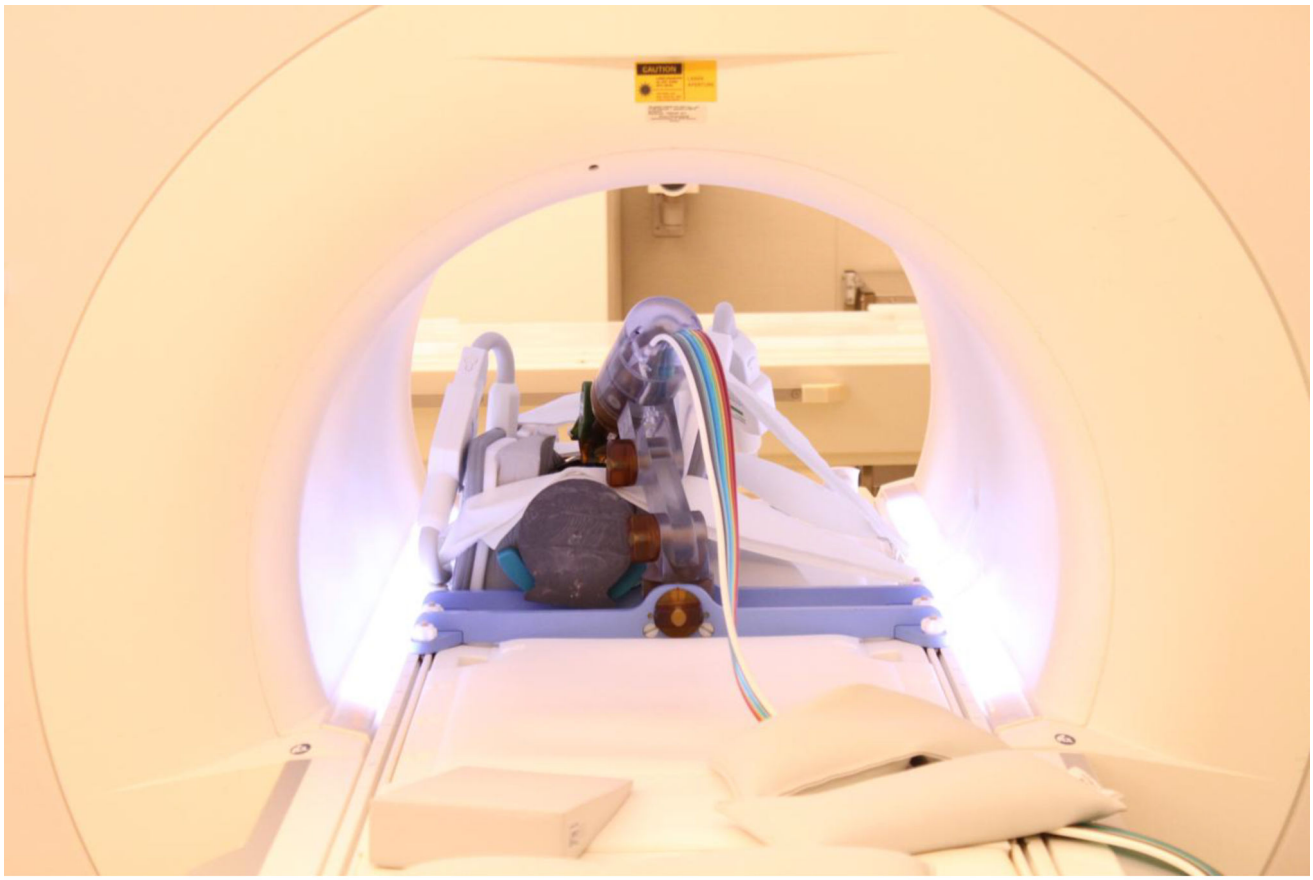

C

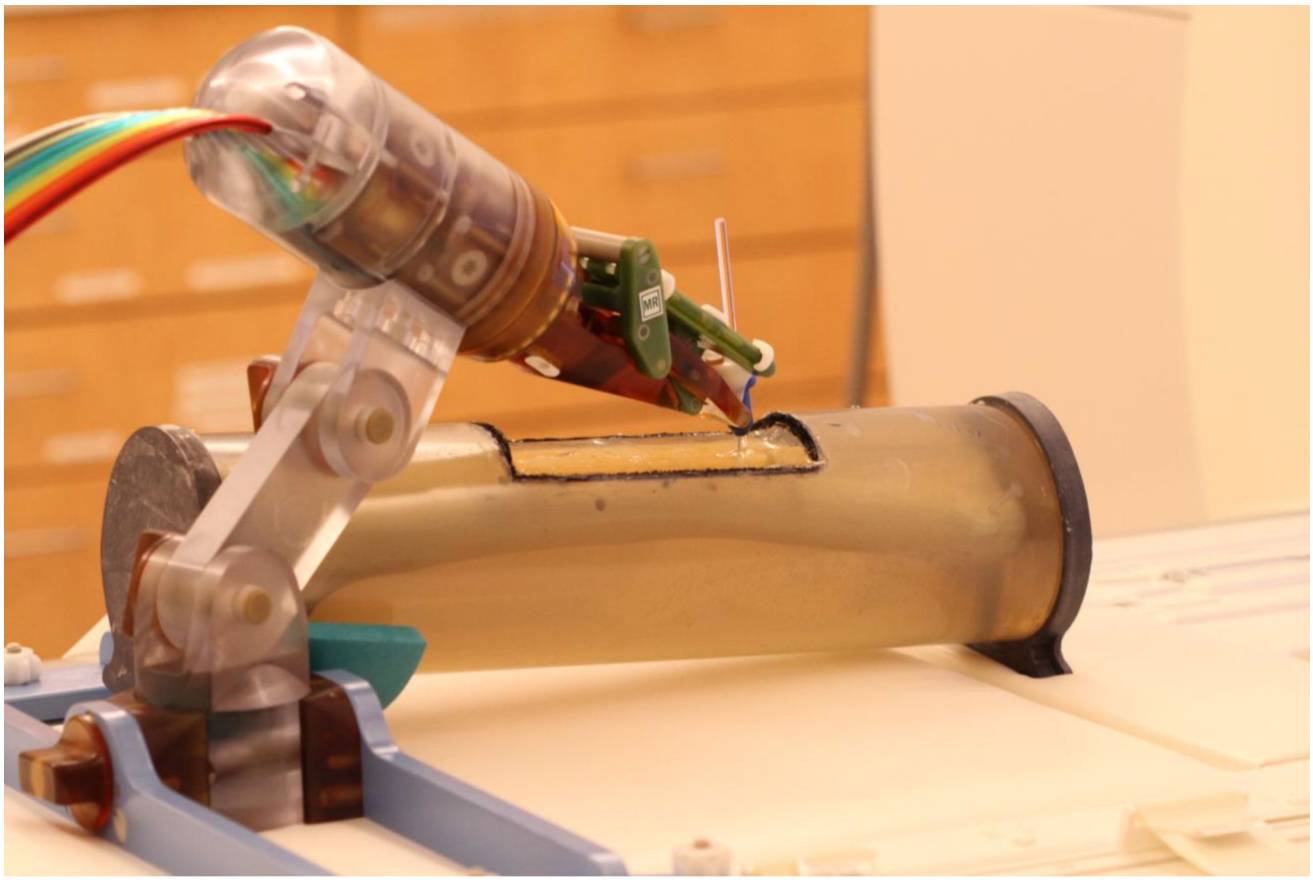

D

Figure 2.

A. Robot mounted on table with long bone phantom in middle and imaging coils on both sides

B. Coils removed to show phantom, robot, and long thin fiducial in needle guide (cutout in phantom

C. Robot in scanner isocenter. Robot can be actuated to align needle guide while at isocenter. View from right side illustrating robot mount and simulated positioning between legs.

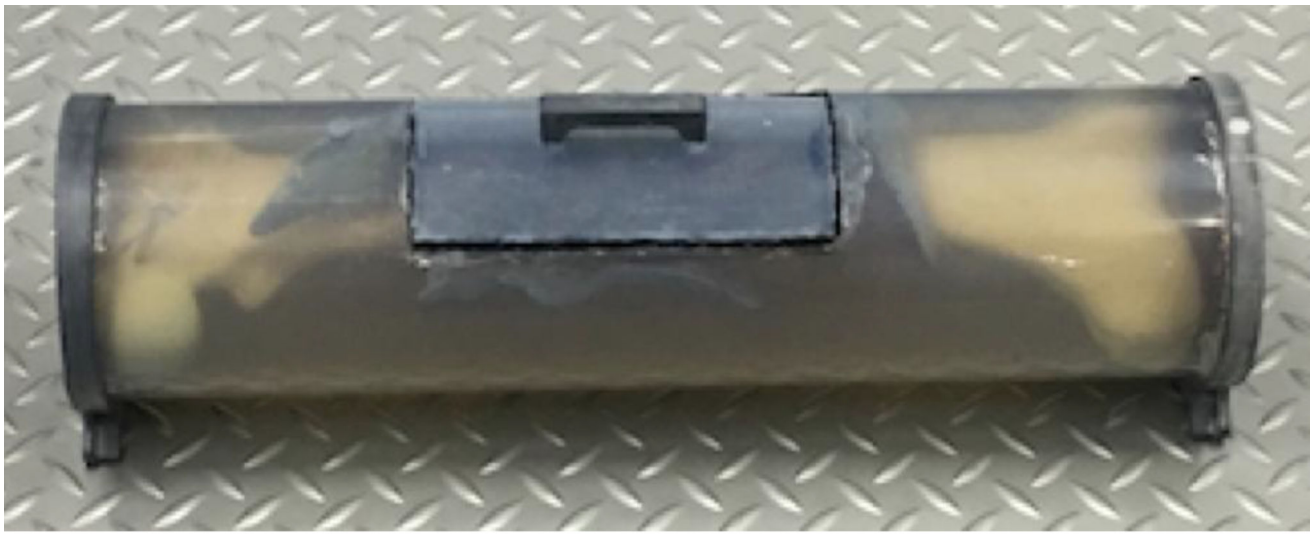

A

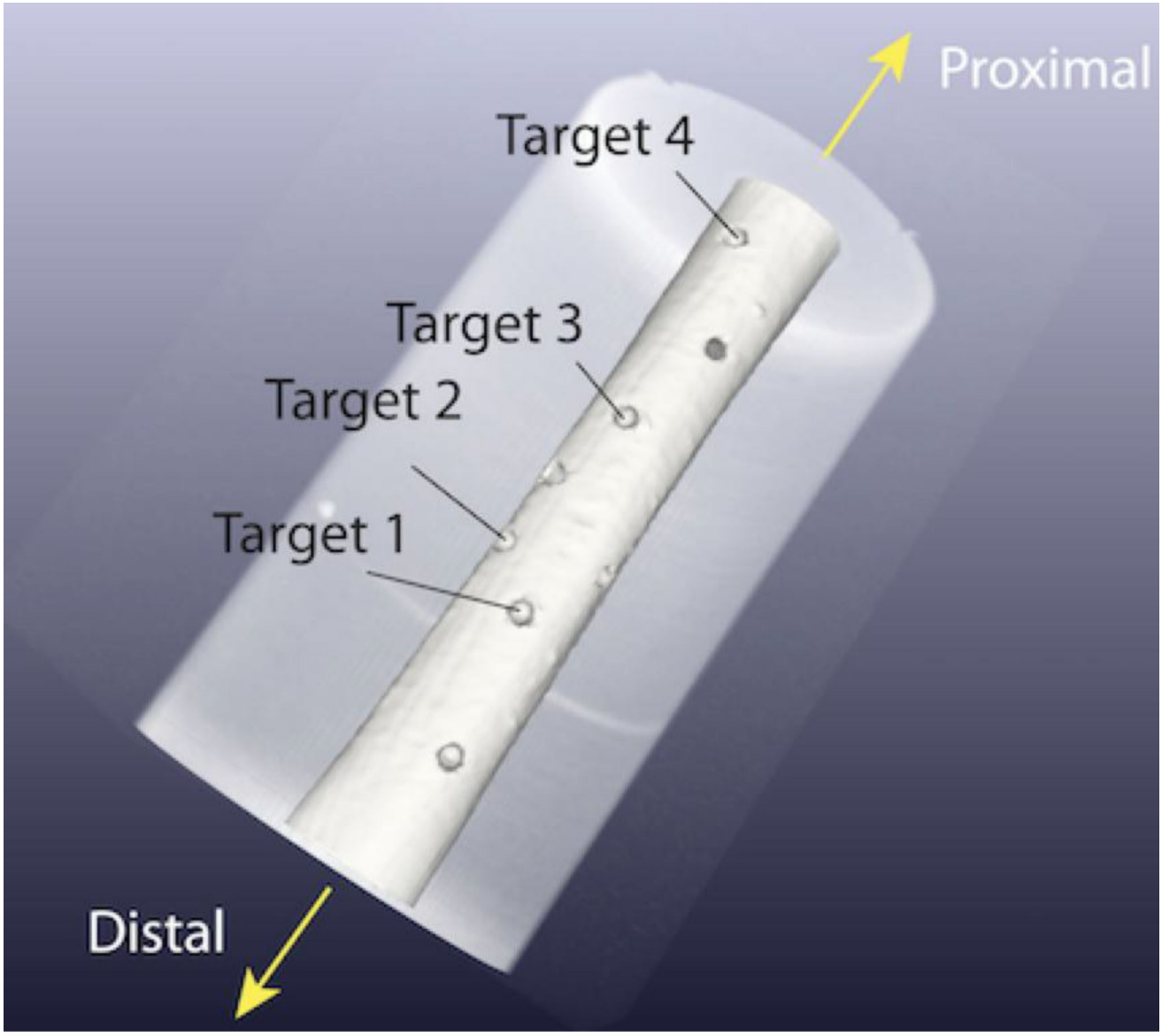

Figure 3.

A. Long bone phantom consists of a sawbones femur model encased in gelation. Cutout on top with handle is removed for targeting experiments.

B. Four targets used in experiments were placed in the area of the cutout. The robot was positioned at the distal end.

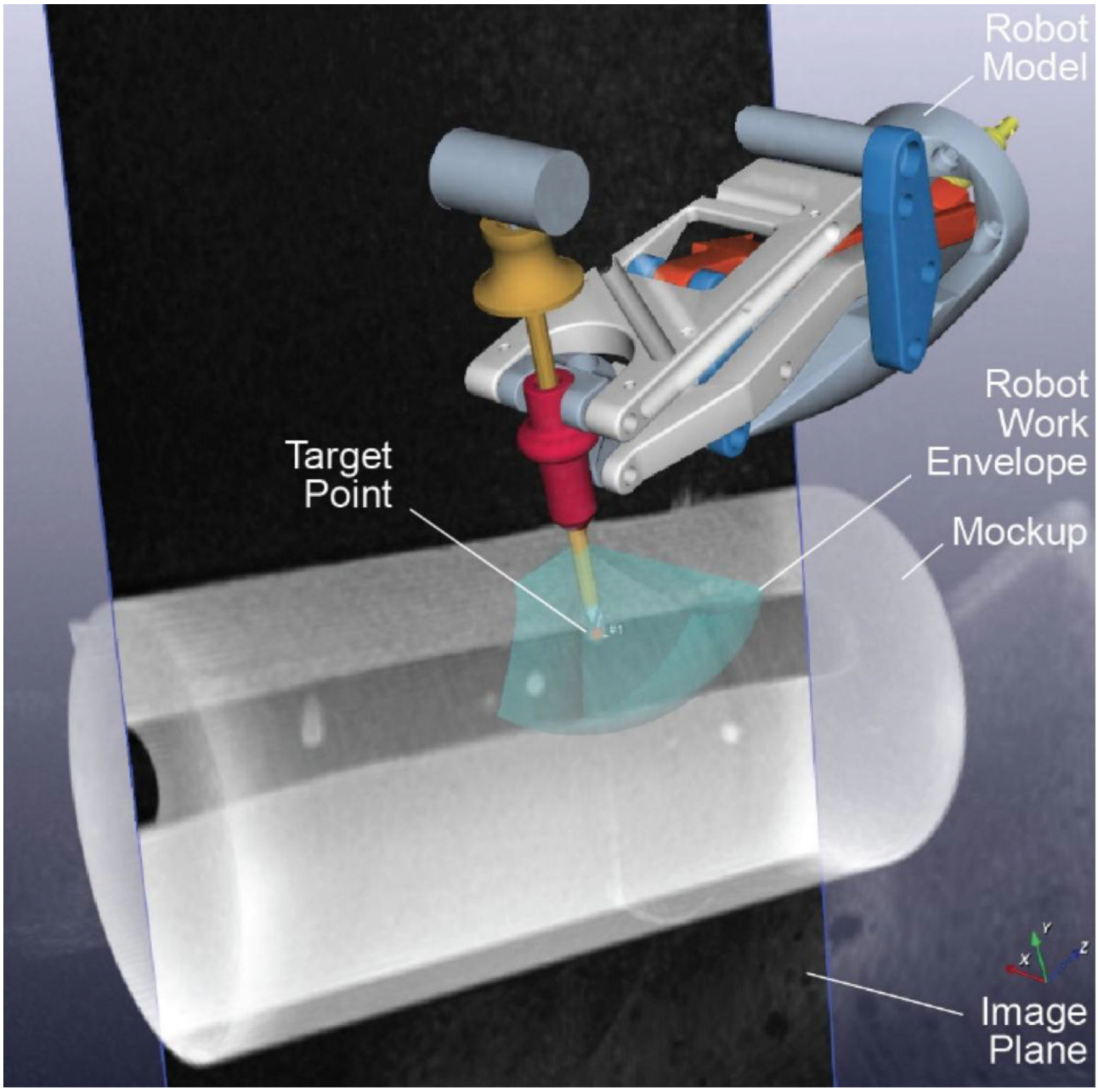

A

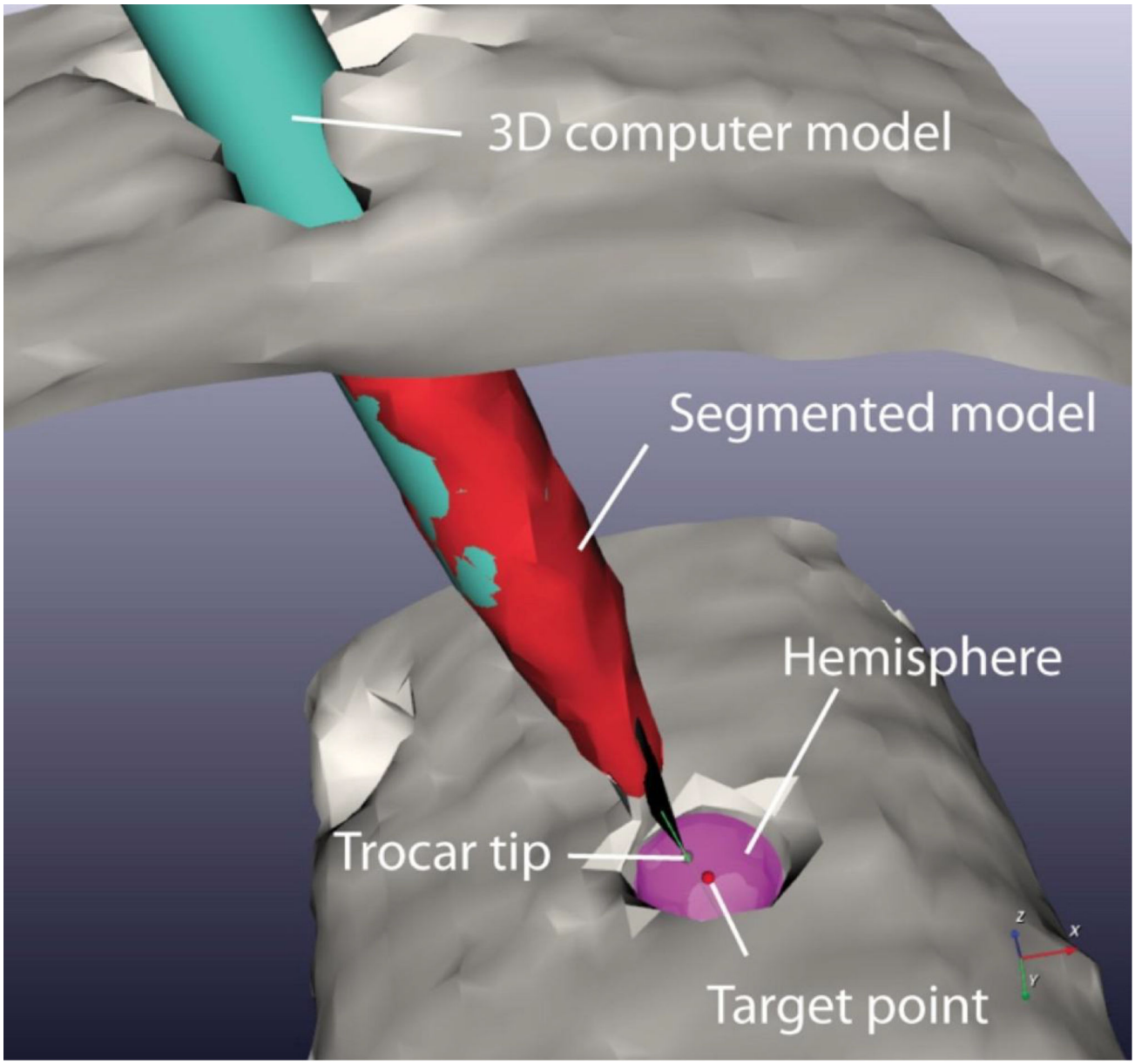

B

Figure 4.

A. 3D model of the robot registered to the image space and with tip of needle at target point (target 1 trial 1).

B. Segmentation of acrylic trocar. The segmented model is in red and the 3D CAD model is in cyan. The green dot is the trocar point and the red dot is the target (target 1 trial 1).

Table 1

Categories of related MRI compatible robots

Category Type	Subcategory	References
Clinical application	Needle-based procedures	[6][7][8]
	Rehabilitation	[9][10]
Mounting method	Patient-mounted	[11][12]
	Bed-mounted	[13][14]
Actuation method	Pneumatic / hydraulic	[15][17][18]
	Piezoelectric motor	[16]
MR Classification: ASTM F2503	MR Conditional	[19][20]
	MR Safe	[7][8][21]

Table 2

Time required for each targeting attempt (all numbers in minutes, first four rows are estimates, last five rows are from DICOM time stamps)

Experiment	1				2				Average	Standard Deviation
Test	**1**	**2**	**3**	**4**	**1**	**2**	**3**	**4**		
Robot and Mockup Mounting on MR table (approx.)	5				5				5	0
Robot cable connection and Robot Homing (approx.)	6				6				6	0
Robot Positioning with RCM at skin entry point (approx.)	5				5				5	0
MR Coil Placement (approx.)	3				3				3	0
MRI Scan for Registration	3.78	3.78	2.27	2.27	3.80	3.78	3.78	3.78	3.41	0.70
Image-Robot Registration	3.05	3.25	3.50	3.38	3.77	3.52	3.35	3.57	3.42	0.22
Robotic orientation of Needle-Guide on target and setting the depth of needle insertion	0.72	1.13	0.65	0.80	0.65	0.87	1.17	1.00	0.87	0.21
Manual Needle Insertion (approx.)	2.50	2.50	2.50	2.50	2.50	2.50	2.50	2.50	2.50	0
MRI Scan for targeting error measurement	2.85	2.77	2.28	2.30	3.78	3.78	3.78	3.78	3.17	0.67
Total Time	**31.90**	**32.43**	**30.20**	**30.25**	**33.50**	**33.45**	**33.58**	**33.63**	**32.37**	**1.46**

Table 3

Results from 8 Targeting Trials

Target	Trial	Target depth [mm]	Needle insertion angle [deg]		2D Error [mm]	3D Error [mm]
			Medial-Lateral	Superior-Inferior		
1	1	27.34	18.86	−11.22	1.17	1.25
	2	21.69	28.60	2.74	0.67	0.69
2	1	30.14	−6.52	16.97	1.50	1.68
	2	26.23	−7.06	−6.55	1.31	1.51
3	1	26.74	18.92	−10.43	1.35	1.35
	2	22.20	−10.10	7.72	0.69	1.01
4	1	28.02	6.72	2.88	1.58	1.71
	2	26.29	−4.40	9.81	1.72	1.89
				MAX	1.72	1.89
				AVERAGE (Accuracy)	1.25	1.39
				STDDEV (Precision)	0.39	0.40